Journal of Solid State Chemistry **155,** 312–319 (2000)
doi:10.1006/jssc.2000.8919, available online at http://www.idealibrary.com on IDEAL®

Structures and Physical Properties of Films Deposited by Simultaneous DC Sputtering of ZnO and In_2O_3 or ITO Targets

Toshihiro Moriga,[1] Takashi Okamoto, Kazunori Hiruta, Azumi Fujiwara, and Ichiro Nakabayashi

Department of Chemical Science and Technology, Faculty of Engineering, University of Tokushima, 2-1 Minami-Josanjima, Tokushima 770-8506, Japan

and

Kikuo Tominaga

Department of Electric and Electronic Engineering, Faculty of Engineering, University of Tokushima, 2-1 Minami-Josanjima, Tokushima 770-8506, Japan

Received April 24, 2000; in revised form July 19, 2000; accepted August 9, 2000; published online November 29, 2000

Oxide films in the ZnO–In_2O_3 and ZnO–tin-doped indium oxide (ITO) systems were deposited by simultaneous dc sputtering of ZnO and In_2O_3 or ITO facing targets at substrate temperatures from room temperature up to 300°C. The ratio δ of the ZnO target current to the sum of both the currents was varied. The bixbyite-type In_2O_3 phase, an amorphous phase, the homologous $Zn_kIn_2O_{k+3}$ phases, and the wurtzite-type ZnO phase were found in this order with increasing δ values. Characteristic trends were observed for δ-dependent electrical properties within the respective phase groups, regardless of the substrate temperatures. The minimum resistivity of $2.3\times10^{-4}\,\Omega$ cm and the maximum carrier concentration of 1.2×10^{21} cm^{-3} were obtained for the amorphous film deposited at 150°C and $\delta = 0.20$, having the atomic ratio of [Zn]/([In]+[Zn]) = 0.22. Sn doping was effective in improving the electrical properties only in the region where the bixbyite-type In_2O_3 phase appeared and was less effective in the amorphous, homologous $Zn_kIn_2O_{k+3}$ and wurtzite-type ZnO regions. © 2000 Academic Press

Key Words: **transparent conducting oxides; dc sputtering with facing targets system; amorphous films; Sn-doping effects.**

INTRODUCTION

At present Sn-doped indium oxide (ITO) films are widely used for optical devices. However, other materials such as ZnO doped with Al, Ga, and In have been investigated with the aim of fabricating transparent conducting oxide (TCO) films having superior electrical, optical, and/or chemical properties and of finding less expensive materials with lower resistivity and higher transmittance (1–4). In the present study, we focused on TCO films consisting of pseudobinary compounds in the ZnO–In_2O_3 system. This system has been investigated by Kasper (5), Kimizuka *et al.* (6, 7), Minami *et al.* (8,9), Koumoto *et al.* (10–12), and our group (13–15). ZnO and In_2O_3 react at high temperature (>1000°C) to form a series of homologous compounds, $Zn_kIn_2O_{k+3}$, where k is an integer. Kasper demonstrated the formation of the compounds with $k = 2$–5 and 7 at 1100–1550°C (5). However, Kimizuka *et al.* (6) and our group (13) reported that $Zn_3In_2O_6$ is the smallest-k member of the homologous series $Zn_kIn_2O_{k+3}$ in the bulk system. Minami *et al.* reported that resistivities as low as $3.5\times10^{-4}\,\Omega$ cm could be obtained for films whose composition was supposed to be $Zn_2In_2O_5$, sputtered from polycrystalline targets containing 10–60 at.% zinc (9). Continuous structural variation from $Zn_3In_2O_6$ to $Zn_2In_2O_5$ was observed on the films deposited by RF sputtering from $Zn_3In_2O_6$ target with increasing substrate temperature (15). The $Zn_3In_2O_6$ and $Zn_2In_2O_5$ films showed resistivities of $9.5\times10^{-4}\,\Omega$ cm and of $5.0\times10^{-4}\,\Omega$ cm, respectively. The value for $Zn_3In_2O_6$ film is higher by almost one magnitude than that for bulk $Zn_3In_2O_6$. We can anticipate that the higher concentration of oxygen vacancies would exist in the film sample.

Carrier electrons in TCO materials are mainly formed by two mechanisms. One is due to oxygen vacancies. One oxygen vacancy produces two carrier electrons theoretically according to the following reaction: $O_0^x \rightarrow 1/2O_2(g) + V_0^{\cdot\cdot} + 2e'$. The other is due to partial substitution of aliovalent cations for the matrix cations. The presence of tin in ITO films creates carrier electrons. Low resistivity ITO films were obtained when 10 wt% of SnO_2 was doped into In_2O_3 matrix (16, 17).

In this paper, we deposited oxide films of ZnO–In_2O_3 by simultaneous sputtering of ZnO and In_2O_3 targets in a facing targets system, over a wide range of applied current ratios of the targets, and investigated their electrical and

[1] To whom correspondence should be addressed. E-mail: moriga@chem.tokushima-u.ac.jp. Fax: +81-88-655-7025.

0022-4596/00 $35.00

optical properties compared with the phases produced. Also, we tried similar experiments using an ITO target instead of the In_2O_3 target to examine the Sn-doping effect on the properties of films in the ZnO–In_2O_3 system.

EXPERIMENTAL

The sputtering apparatus used in this experiment is shown in Fig. 1. Two ceramic disk targets of ZnO and In_2O_3 (or ITO), 10 cm in diameter and 5 mm in thickness, facing each other, were sputtered simultaneously using a dc magnetron sputtering method. The ITO target contained 90 wt% In_2O_3 and 10 wt% SnO_2. Each target was held on permanent magnets with opposite polarities to improve the electron confinement between the target faces. A Corning No. 7059 glass substrate $50 \times 50 \times 1$ mm^3 was located beside the targets. The distance between each target was 10 cm and that between the center of the target and the substrate was 10 cm. Prior to deposition, the chamber was evacuated to 1×10^{-5} Torr. Argon gas was then introduced to the chamber to maintain the sputtering atmosphere at a pressure of 1×10^{-3} Torr. After 20 min of presputtering with the shutter closed in front of the substrate, 120 min of deposition was performed. The discharge currents of ZnO and In_2O_3 (or ITO) targets designated as I_{Zn} and I_{In}, respectively, were controlled during deposition of the films. The current ratio was defined as $\delta = I_{Zn}/(I_{Zn} + I_{In})$. When $0 \le \delta \le 0.50$, I_{In} was fixed to be 80 mA and I_{Zn} was varied from 0 to 80 mA. Inversely, when $0.50 \le \delta \le 1.00$, I_{Zn} was fixed to be 80 mA and I_{In} was varied. Films were deposited by changing δ for several substrate temperatures (T_s) of room temperature (without heating the substrate): 150, 250, and 300°C.

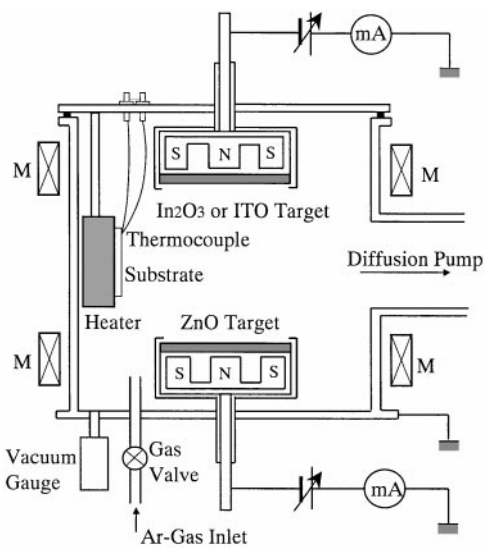

FIG. 1. Schematic drawing of facing-target dc sputtering apparatus. M represents Helmholtz-type coil for confining electrons between the targets.

The T_s without heating increased to ~ 50°C when the deposition was finished.

Phase identification was performed with a powder X-ray diffractometer (Rigaku RINT2500VHF$^+$) using monochromatized Cu$K\alpha$ radiation with a source power of 40 kV and 150 mA. Room-temperature electrical resistivity of the films was measured with a spring-loaded linear four-probe apparatus using a current source and a voltmeter (Advantest R6144 and R6551). The resistivity was calculated as

$$\rho = \frac{V}{I} \cdot \frac{\pi}{\ln 2} w,$$

where ρ is resistivity, V is voltage drop, I is excitation current, and w is film thickness. The film thickness w was measured by a surface roughness detector (DEKTAK 3030). Carrier concentration, n, and Hall mobility, μ_H, were estimated from the measurement of the Hall voltage in a dc magnetic field and dc current applied to the film, which was shaped into a cross (18) (van der Pauw method). The Van der Pauw method is the most suitable one for measuring the Hall voltage of thin samples (19). UV-VIS transmittance was measured using a spectrophotometer (JASCO V500DS). Surface images of the films were observed by field emission scanning electron microscopy (Hitachi S4700). The cation ratio of the films was determined by fluorescent X-ray analysis (Shimadzu EDX-800).

RESULTS AND DISCUSSION

Structural and Electrical Properties of Films in the ZnO–In_2O_3 System

Figures 2a and 2b show X-ray diffraction patterns for the ZnO–In_2O_3 films deposited at $T_s = 150$ and 300°C, respectively, as a function of δ value. For $T_s = 150$°C, the diffraction patterns indicate that the films were composed of the bixbyite-type In_2O_3 in the range of $0 \le \delta \le 0.11$. No preferred orientation was noted. In the δ range from 0.20 to 0.57, amorphous-like films with a broad peak at $2\theta \simeq 32^\circ$ were obtained. The scales of diffraction intensities for the samples $\delta = 0.20$, 0.33, 0.50, and 0.57 in Fig. 2a were magnified by 8–10 times, compared with the scales for $\delta = 0.00$ and 1.00. The broad peak shifted to the higher 2θ values with increasing δ values, which results from increasing zinc content in the film. A Zn^{2+} ion has a smaller ionic radius than an In^{3+} ion (20). At $\delta = 0.66$, several peaks assigned to one of the homologous compounds, $Zn_5In_2O_8$, appeared. In the δ range from 0.80 to 1.00, all peaks observed were assigned to the wurtzite-type ZnO. The film deposited at $\delta = 1.00$ had a strong preferred c-axis orientation whereas the diffraction pattern for $\delta = 0.80$ was similar to a bulk ZnO with a slight shift to the lower 2θ side due to occlusion of the larger In^{3+} ions. For $T_s = $ RT, amorphous-like films were

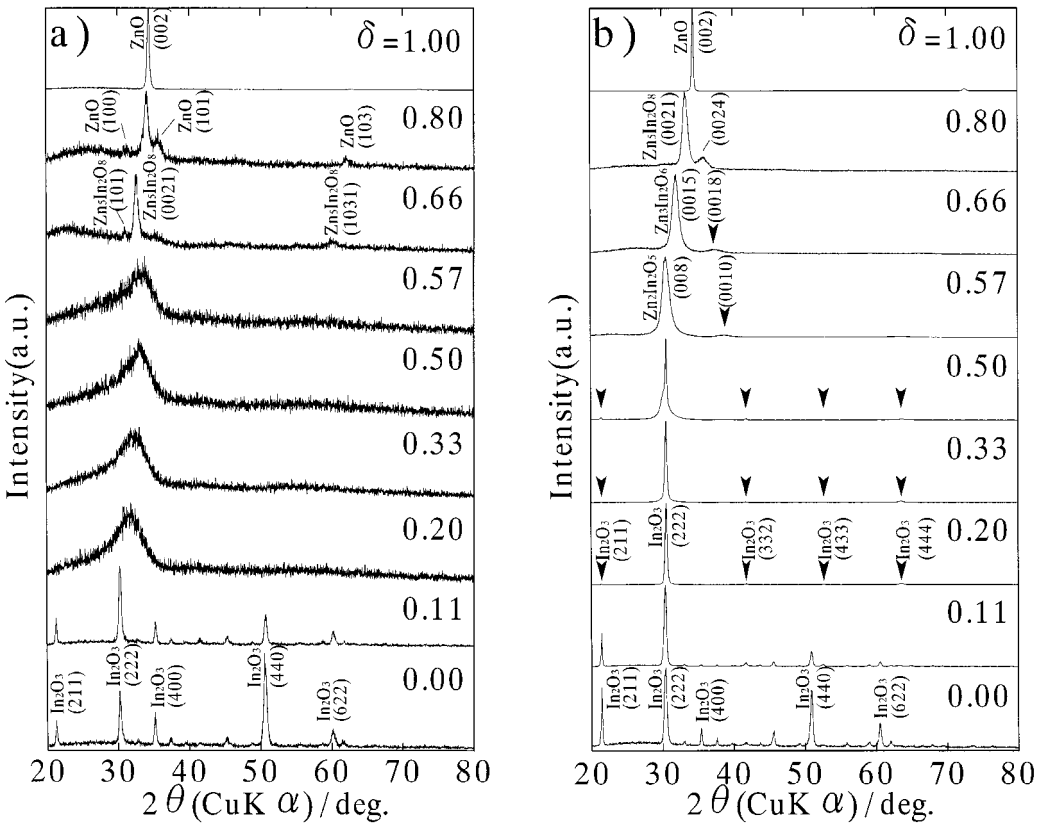

FIG. 2. X-ray diffraction patterns for ZnO–In_2O_3 films deposited at (a) $T_s = 150°C$ and (b) $T_s = 300°C$ as a function of δ value. The scales of diffraction intensities for the samples of $\delta = 0.20$, 0.33, 0.50, and 0.57 in (a) were magnified by 8–10 times, compared with the scales for $\delta = 0.00$ and 1.00. Arrows represents the positions of faint peaks observed.

obtained in a wider δ range from 0.11 to 0.66. No homologous compounds, $Zn_kIn_2O_{k+3}$, could be detected.

Drastic changes were observed in the phase composing the films deposited at $T_s = 300°C$. At $\delta = 0.00$ and 0.11, the films were composed of In_2O_3, but the position of the strongest diffraction peak did not shift up to $\delta = 0.50$. X-ray fluorescence indicated that the films at $\delta = 0.50$ contained as little as 35 at.% zinc on a cation basis. Of interest, several very small peaks could be detected in the films for $\delta = 0.20$, 0.33, and 0.50 by magnifying the ordinate. The peaks at $2\theta \simeq 21.5°$, 30.5°, 41.8°, 52.7°, and 63.7° were assigned to (2 1 1), (2 2 2) (this peak is the strongest), (3 2 2), (4 3 3), and (4 4 4) reflections of the bixbyite-type In_2O_3, respectively. A (1 1 1)-preferred orientation is noted. As the bixbyite-type In_2O_3 has the space group $Ia3$, the reflections with all-odd indexes such as (1 1 1) and (3 3 3) do not appear because of the extinction law. The reason why they should be in the (1 1 1)-orientation is not clear. It is possible that the films might have one of the superstructures of the bixbyite.

The strongest peak at $2\theta \simeq 31°$ was broadened and shifted toward the higher 2θ side with increasing δ value ($\delta = 0.57$, 0.66, and 0.80). In this δ range, the second strongest (but broad) peak shifted to the lower 2θ side. The strongest and second strongest peaks were approaching each other with increasing δ value, and they seemed to overlap at the (0 0 2) peak of the wurtzite-type ZnO at $\delta = 1.0$. This kind of peak shift implies that the homologous compounds $Zn_kIn_2O_{k+3}$ were formed in the films at $\delta = 0.75$, 0.66, and 0.80 (13), and the k number of the compound increased with increasing δ value, i.e., with increasing zinc content. Considering the strongest peak position, the main component of the films at $\delta = 0.57$, 0.66, and 0.80 would be $Zn_2In_2O_5$, $Zn_3In_2O_6$, and $Zn_5In_2O_8$, respectively. The strongest peak indices for the respective compounds are (0 0 8) of $Zn_2In_2O_5$, (0 0 $\underline{1}$ 5) of $Zn_3In_2O_6$, and (0 0 $\underline{2}$ $\underline{1}$) of $Zn_5In_2O_8$ and the second strongest peaks indexed are (0 0 $\underline{1}$ 0), (0 0 $\underline{1}$ 8), and (0 0 $\underline{2}$ 4). These facts suggest that these films have the c-axis-preferred orientation. The broadness of the peaks would be due to stacking faults between homologous compounds $Zn_kIn_2O_{k+3}$ with the corresponding k number and those with the $(k+1)$ and/or $(k-1)$ compounds. For $T_s = 250°C$, the bixbyite-type In_2O_3 phase appeared for the films of $\delta = 0.00$ and 0.11. The oriented In_2O_3 phase was detected at $\delta = 0.20$. At around $\delta = 0.33$, a biphasic sample of an amorphous phase and the oriented In_2O_3 could be obtained. Homologous

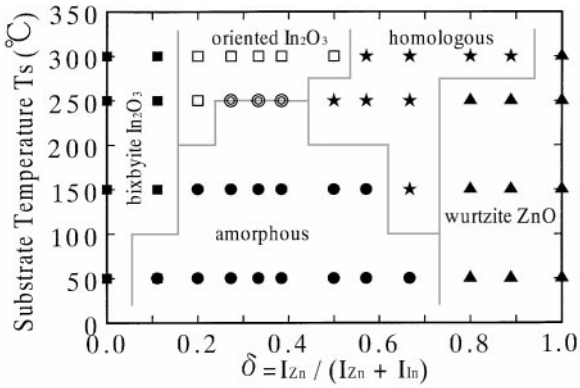

FIG. 3. Phases observed for ZnO–In_2O_3 films as functions of $\delta = I_{Zn}/(I_{Zn} + I_{In})$ and substrate temperature, T_s. (■) Bixbyite-type In_2O_3, (□) oriented In_2O_3, (●) amorphous, (★) homologous $Zn_kIn_2O_{k+3}$, (▲) wurtzite-type ZnO, and (●) mixture (amorphous + oriented In_2O_3).

compounds of $Zn_2In_2O_5$ and $Zn_3In_2O_6$ were observed in the films of $\delta = 0.50$ and 0.66, respectively. In the δ range above 0.80, we could assign the films to the wurtzite-type ZnO. Considering the X-ray diffraction results, T_s and δ value strongly govern the phases observed in the films. Figure 3 shows the phase(s) observed for the films in this experiment. At the low T_s (≤ 150°C), an amorphous phase appears and the oriented In_2O_3 phase could not be detected. The higher T_s leads to the wider In_2O_3 region (including the oriented phase region) and the homologous $Zn_kIn_2O_{k+3}$ region.

Figure 4 represents δ-value dependence of film thickness deposited at 150 and 300°C, respectively. The thickness varied with δ value. The maximum thickness was noted at $\delta = 0.50$ for both substrate temperatures due to the manners in which current was applied (see Experimental section). The film thickness deposited at 300°C is about 30% thinner than that deposited at 150°C. The deposited atoms have a higher activity at the higher temperature, resulting in resputtering and/or rearrangement of atoms to form the dense structure. SEM images of the films deposited at 150 and 300°C, with $\delta = 0.20$, are shown in Figs. 5a and 5b, respectively. The amorphous film (Fig. 5a) was made up of spike-like grains of $\sim$1000 Å whereas the oriented-In_2O_3 film (Fig. 5b) was made up of plate-like grains. It can easily be understood that this film should have a preferred orientation.

Electrical properties for the films deposited at RT, 150°C, and 300°C are shown in Figs. 6a, 6b, and 6c. All the films

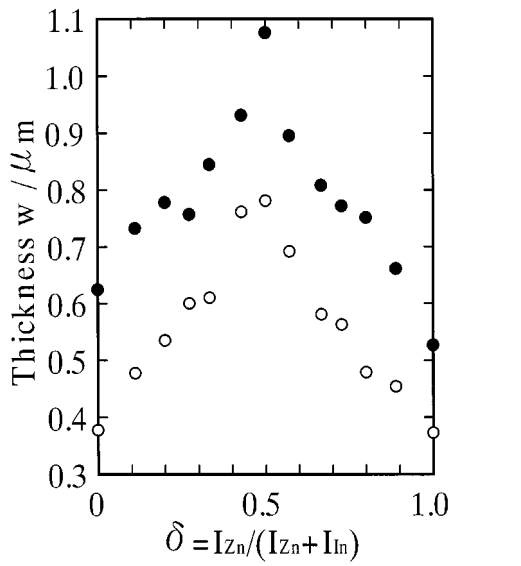

FIG. 4. The δ-value dependence of ZnO–In_2O_3 film thickness deposited at 150°C (●) and 300°C (○).

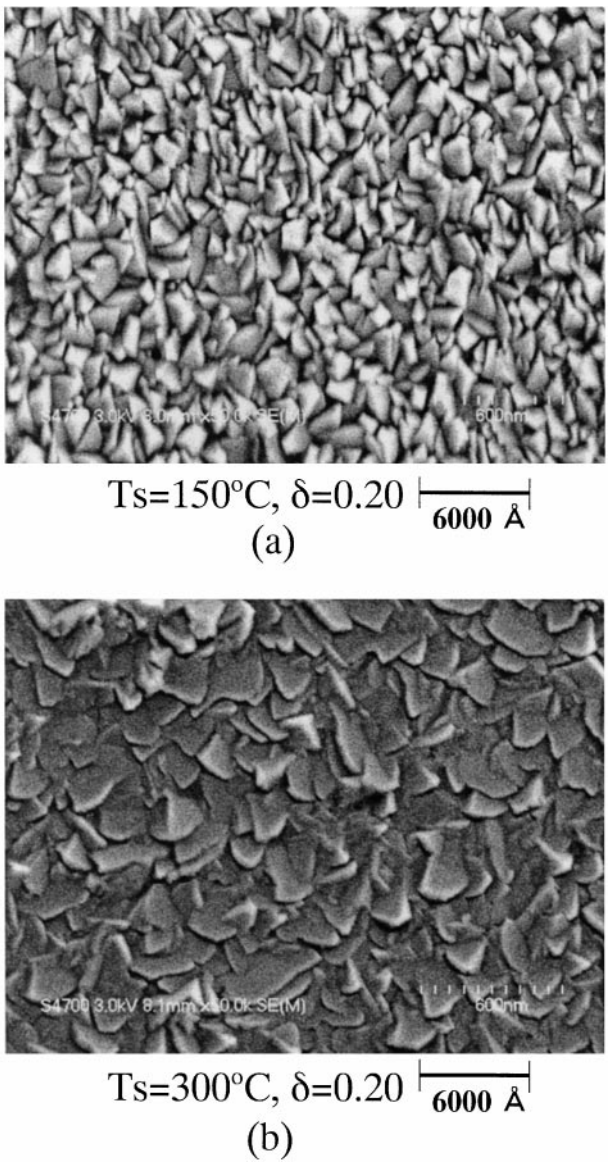

FIG. 5. SEM images of the films deposited at (a) 150°C and (b) 300°C, with $\delta = 0.20$.

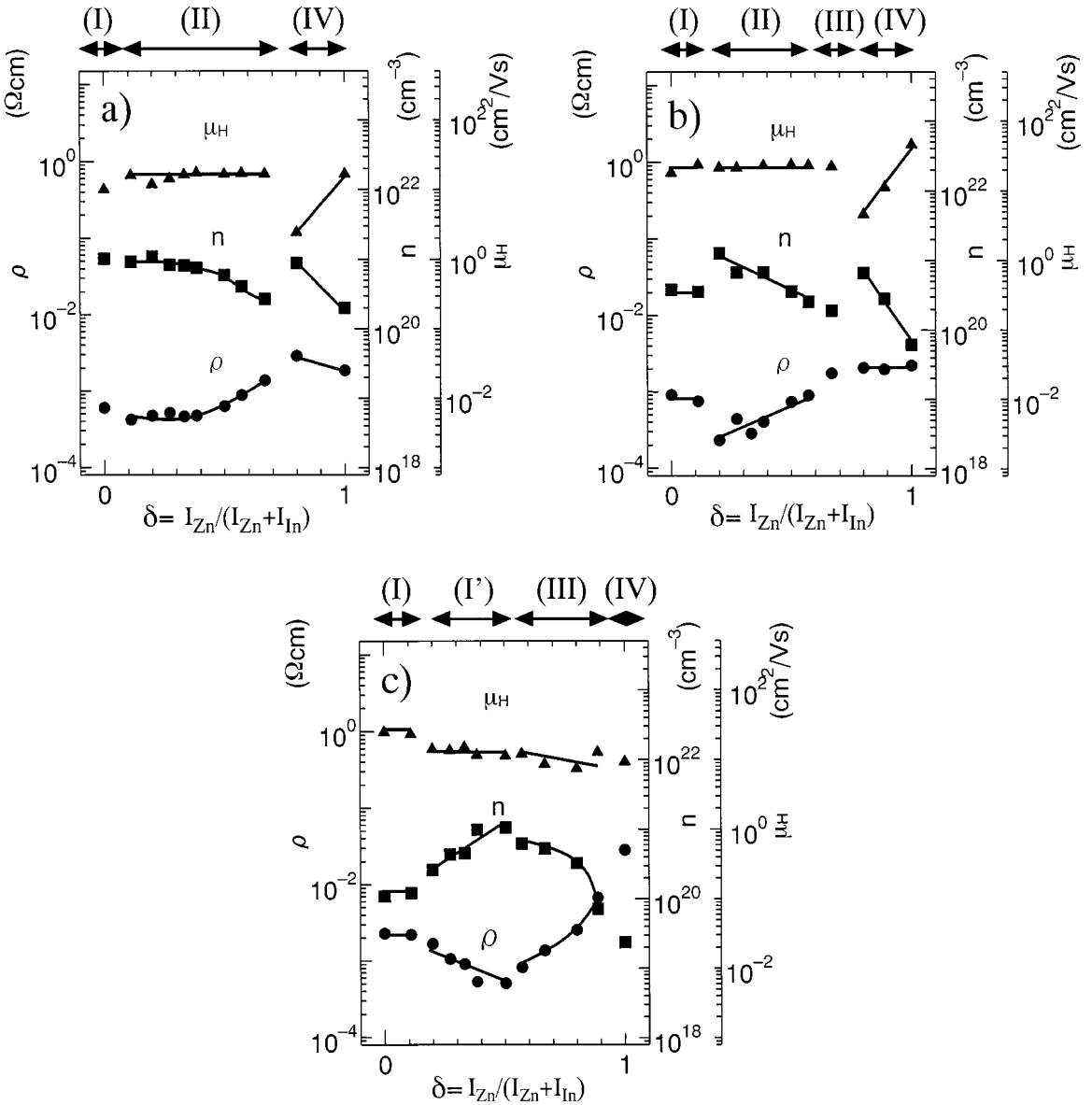

FIG. 6. Electrical properties for $ZnO–In_2O_3$ films deposited at (a) RT, (b) 150°C, and (c) 300°C, as a function of the current ratio δ. Notations (I), (I′), (II), (III), and (IV) represent observed phase. (I) Bixbyite-type In_2O_3, (I′) oriented In_2O_3, (II) amorphous, (III) homologous $Zn_kIn_2O_{k+3}$, and (IV) wurtzite-type ZnO.

showed *n*-type conductivity. Resistivity, Hall mobility, and carrier concentration varied in complex ways with the δ value. However, some trends can be observed when these parameters are classified by the phases formed in the films. The plots of the respective parameters are joined by a smooth line for each phase in Figs. 6a–6c. Resistivity, mobility, and carrier concentration were all unchanged in the δ range (I) where the polycrystalline bixbyite-type In_2O_3 was formed. Resistivity and mobility decreased and carrier concentration was almost constant with increasing δ value in region I′ where the oriented In_2O_3 phase was formed. Resistivity increased, mobility was almost constant, and carrier concentration decreased in region II where the amorphous phase was formed. Resistivity increased, while mobility and carrier concentration decreased in region III where homologous compounds $Zn_kIn_2O_{k+3}$ were formed. This trend seen in region III is in good agreement with that reported in our bulk work (13); resistivity increased as *k* number increased because of decreased carrier concentration as well as decreased mobility. In region IV where the wurtzite-type ZnO was formed, resistivity was almost constant or slightly decreased, mobility increased, and carrier concentration decreased. The minimum resistivity of $2.3 \times 10^{-4}\ \Omega$ cm and the maximum carrier concentration of

1.2×10^{21} cm^{-3} were obtained for the amorphous film ($\delta = 0.20$) deposited at 150°C. The resistivity is equal to that of ITO films (16, 17, 21). The atomic ratio of cations ($Zn/[In + Zn] = 0.22$) in the film having the minimum resistivity, which was determined by X-ray fluorescent analysis, was the same as the ratio estimated from the applied current ratio within experimental errors. We could obtain a highly conductive material under conditions of lower T_s with a lower amount of expensive indium.

Sn-Doping Effects for the Films Deposited at 150°C (ZnO–ITO System)

As mentioned in the Introduction, Sn doping is effective for improving electrical properties of the bixbyite-type In_2O_3, which is well known as ITO. Phillips *et al.* reported that sputtered amorphous-like $Zn_xIn_yO_z$:Sn films with compositions of $[Zn]/([In] + [Sn]) = 0.5–0.6$ (i.e., $[Zn]/([Zn] + [In]) \simeq 0.33–0.375$) showed a resistivity of 3.8×10^{-4} Ω cm (22). Though they did not refer to the amount of tin present in the films, they inferred that the Sn is an effective dopant to such amorphous films. In this section, we examine the doping effect in thin films, especially amorphous films, by comparing the films in the ZnO–In_2O_3 system with those in the ZnO–ITO system.

Figure 7 shows X-ray diffraction patterns for ZnO–ITO films deposited at $T_s = 150$°C as a function of δ value. The features of diffraction patterns did not change much compared with the case of the ZnO–In_2O_3 films. The region of amorphous phase became a bit narrower. At $\delta = 0.57$, the homologous compound $Zn_3In_2O_6$ appeared. Figure 8 shows the variation of electrical properties for ZnO-ITO films deposited at $T_s = 150$°C. Carrier concentration decreased with increasing zinc concentration over the entire amorphous region, whereas Hall mobility was unchanged, so that resistivity was increased. A resistivity of 4.5×10^{-4} Ω cm was obtained for the film at $\delta = 0.2$ for the ZnO–ITO system, which is two times larger than that for the ZnO–In_2O_3 system. The electrical characteristics of the amorphous films did not increase with Sn doping as expected. While low-level doping with aliovalent cations often results in remarkable increases in conductivity (23, 24), the electrical data suggest that oxygen vacancies are the primary electron donors in the amorphous films. The characteristic δ-value dependence of these electrical properties in the ZnO–ITO films, which has been seen in the amorphous, the homologous $Zn_kIn_2O_{k+3}$, and the wurtzite-type ZnO regions, was virtually identical to that of the ZnO–In_2O_3 films. However, the trend changed in the bixbyite-type In_2O_3 region. The film at $\delta = 0.0$, i.e., pure ITO film, had a resistivity of 3.5×10^{-4} Ω cm. This value is compatible with the values reported in the previous papers (16, 17, 21). Sn-doping caused increased carrier concentration and decreased Hall mobility. Though the Sn doping lowered the values of resistivity, the magnitude of lowered resistivity decreased with increasing δ value.

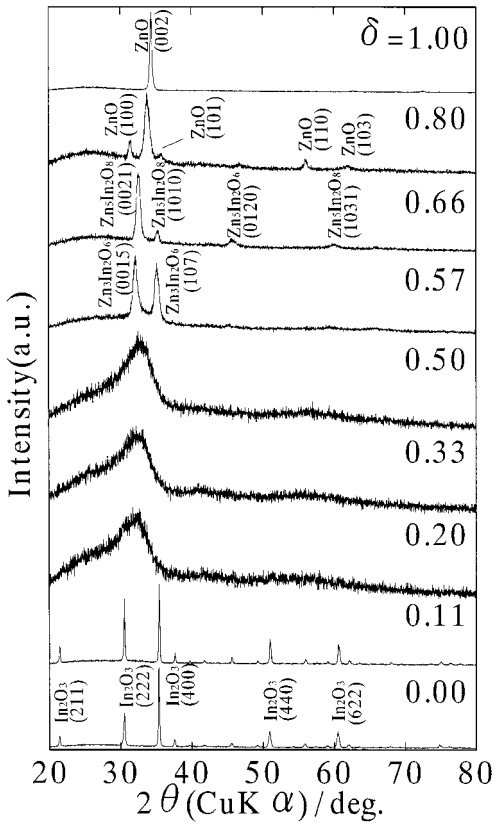

FIG. 7. X-ray diffraction patterns for ZnO–ITO films deposited at $T_s = 150$°C as a function of δ value.

The difference in carrier concentrations could also be seen in the optical properties. Figure 9 shows optical transmission spectra for the films deposited at $T_s = 150$°C. First, we consider the optical properties of the films with the bixbyite-type structure. The ITO film ($\delta = 0.0$; indium source, ITO) had the widest band gap of ~4.1 eV. This value is compatible with the values reported in the previous papers (16, 17, 21). The film of $\delta = 0.11$ deposited using the ITO target as an indium source showed a lower band gap (~3.9 eV) and a higher transmittance in the high wavelength region (above 600 nm) than the ITO film. Increased resistivity correlates with lower band gap. Burstein showed that in degenerate semiconductors with curved bands, filling of states caused a widening of the direct optical band gap (Burstein–Moss shift) (25). This explanation supports our electrical data. Palmer *et al.*, proposed that donor–acceptor pairs formed from Zn^{2+} and Sn^{4+} caused band gap narrowing in bulk ZnO/SnO_2-cosubstituted In_2O_3 (26). Our films also contain Zn^{2+} and Sn^{4+} ions. The Zn^{2+}/Sn^{4+} pairs would offset the effect of conduction carriers, so that the carrier concentration of the film of $\delta = 0.11$ decreased compared with that of the ITO film.

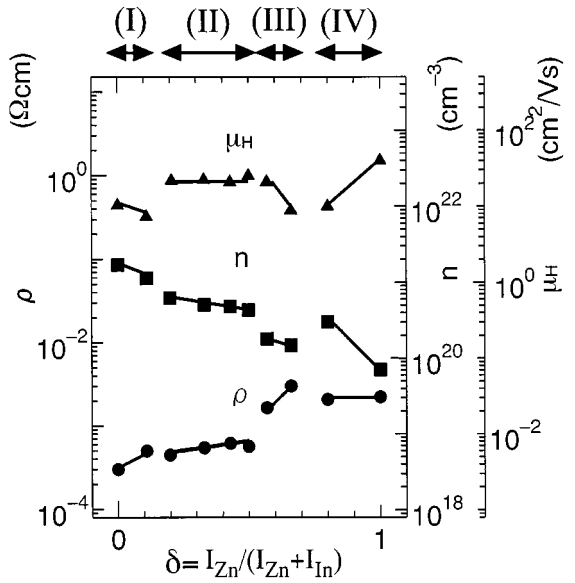

FIG. 8. Electrical properties for ZnO–ITO films deposited at 150°C, as a function of the current ratio δ. Notations (I), (I′), (II), (III), and (IV) are the same as in Fig. 6.

Concerning the amorphous films ($\delta = 0.20$), the observed band gaps (3.6 eV for the $ZnO–In_2O_3$ system and 3.5 eV for the ZnO–ITO system) and the transmittance seemed to be almost identical despite the difference of the indium source. Carrier concentration by Hall measurements for the ZnO–ITO film was larger by two times than that for the $ZnO–In_2O_3$ film (see Figs. 6b and 6c). Granqvist *et al.*, showed that the calculated Burstein–Moss shift band gap widening was partially offset by band gap narrowing from many-body interactions in some TCOs (27–29). Shimakawa *et al.*, found that in amorphous TCO films in the $CdO–GeO_2$ system the number of carriers participating in the free carrier absorption is larger than the number participating in the Hall effect (24). This effect was explained by macroscopic potential fluctuation (modulated band edges) introduced by impurity doping. However, the origin of the band gaps in the *amorphous* films in the $ZnO–In_2O_3–SnO_2$ system is unclear.

In the $ZnO–In_2O_3$ system, it can be clarified that the Sn doping was effective only in the region where the In_2O_3 bixbyite-type phase appeared and was less effective in the amorphous and homologous $Zn_kIn_2O_{k+3}$ regions. The electrical properties of the amorphous and the homologous $Zn_kIn_2O_{k+3}$ phases would be improved by oxygen vacancies donating carriers.

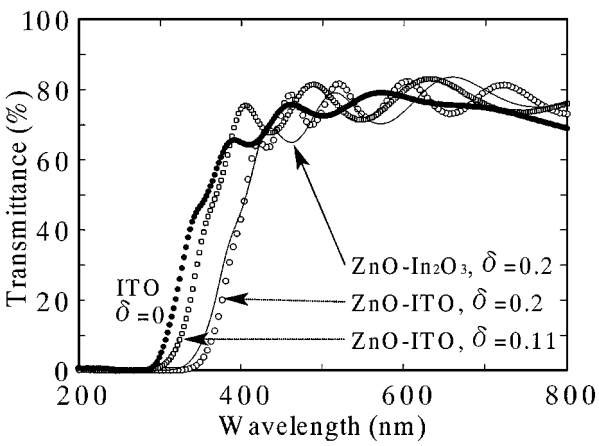

FIG. 9. Optical transmission spectra for the films deposited at $T_s = 150$°C. (Solid line) $ZnO–In_2O_3$ with $\delta = 0.20$, (●) ITO, (□) ZnO–ITO with $\delta = 0.11$, and (○) ZnO–ITO with $\delta = 0.20$.

ACKNOWLEDGMENTS

This work was partly supported by a Grant-in-Aid for Scientific Research from the Ministry of Education, Science, Sports and Culture and also by a research grant from the Satellite Venture Business Laboratory of the University of Tokushima.

REFERENCES

1. K. Tominaga, N. Umezu, I. Mori, T. Ushiro, T. Moriga, and I. Nakabayashi, *J. Vac. Sci. Technol. A* **16,** 1213 (1998).
2. K. Tominaga, T. Murayama, N. Umezu, I. Mori, T. Ushiro, T. Moriga, and I. Nakabayashi, *Thin Solid Films* **343–344,** 160 (1999).
3. R. Wang, L. H. L. King, and A. W. Sleight, *J. Mater. Res.* **11,** 1659 (1996).
4. M. Miyazaki, K. Sato, A. Mitsui, and H. Nishijima, *J. Non-Cryst. Solids* **218,** 323 (1997).
5. V. H. Kasper, *Z. Anorg. Allg. Chem.* **349,** 113 (1967).
6. N. Kimizuka, M. Isobe, and M. Nakamura, *J. Solid State Chem.* **116,** 170 (1995).
7. M. Isobe, N. Kimizuka, M. Nakamura, and T. Mohri, *Acta Crystallogr. C* **50,** 332 (1994)
8. T. Minami, H. Sonohara, T. Kakumu, and S. Tanaka, *Jpn. J. Appl. Phys. Part 2* **34,** L971 (1995).
9. T. Minami, T. Kakumu, and S. Tanaka, *J. Vac. Sci. Technol. A* **14,** 1704 (1996).
10. H. Ohta, W. S. Seo, and K. Koumoto, *J. Am. Ceram. Soc.* **79,** 2193 (1996).
11. H. Hiramatsu, W. S. Seo, and K. Koumoto, *Chem. Mater.* **10,** 3033 (1998).
12. Y. Masuda, M. Ohta, W. S. Seo, W. Pitschke, and K. Koumoto, *J. Solid State Chem.* **150,** 221 (2000).
13. T. Moriga, D. D. Edwards, T. O. Mason, G. B. Palmer, K. R. Poeppelmeier, J. L. Schindler, C. R. Kannewurf, and I. Nakabayashi, *J. Am. Ceram. Soc.* **81,** 1310 (1998).
14. K. Tominaga, T. Murayama, I. Mori, T. Okamoto, K. Hiruta, T. Moriga, and I. Nakabayashi, *Vacuum*, in press.
15. T. Ushiro, D. Tsuji, Y. Aki, K. Murayama, T. Moriga, K. Tominaga, and I. Nakabayashi, "Proceedings of the Fifth International Symposium on Sputtering and Plasma Process (ISSP'99)," pp. 213–214, 1999, submitted for publication.
16. S. Ray, R. Banerjee, N. Basu, A. K. Batabyal, and A. K. Barua, *J. Appl. Phys.* **54,** 3497 (1983).
17. M. Sawada and M. Higuchi, *Thin Solid Films* **317,** 157 (1998).
18. D. C. Look, *J. Electrochem. Soc.* **137,** 261 (1990).
19. L. J. van der Pauw, *Philips Res. Rep.* **13,** 6 (1958).

20. R. D. Shannon, *Acta Crystallogr. A* **32,** 751 (1976).
21. N. R. Lyman, "Proceedings of the Symposium on Electrochromic Materials," Vols. 90–92, pp. 201–231, Electrochemical Society, Princeton, NJ, 1990.
22. J. M. Phillips, R. J. Cava, G. A. Thomas, S. A. Carter, J. Kwo, T. Siegrist, J. J. Krajewski, J. H. Marshall, W. F. Peck, Jr., and D. H. Rapkine, *Appl. Phys. Lett*. **67,** 2246 (1994).
23. H. Hosono and H. Kawazoe, *Mater. Sci. Eng. B* **41,** 39 (1996).
24. K. Shimakawa, H. Hosono, N. Kikuchi, and H. Kawazoe, *J. Non-Cryst. Solids* **227–230,** 513 (1998).
25. E. Burstein, *Phys. Rev*. **93,** 632 (1954).
26. G. B. Palmer, K. R. Poeppelmeier, and T. O. Mason, *Chem. Mater*. **9,** 3121 (1997).
27. I. Hamberg and C. Granqvist, *J. Appl. Phys*. **60,** R123 (1986).
28. Z. Jin, I. Hamberg, and C. Granqvist, *J. Appl. Phys*. **64,** 5117 (1988).
29. B. Sterjna and C. Granqvist, *Thin Solid Films* **193/194,** 704 (1990).